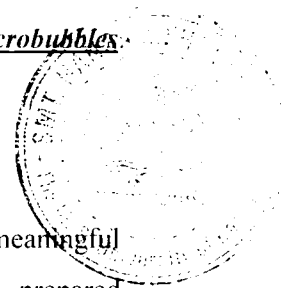# Chapter 6

Characterization of Liposomes and Microbubbles

Preparation, Optimization, and Characterization of 6-Mercaptopurine liposomes, **Journal of Pharmacy and Pharmaceutical Sciences** (Under communication)

And

Perfluorocarbon based microbubbles for delivery of anti-cancer drugs. **Drug Development and Industrial Pharmacy**, (Under communication)

6.1 INTRODUCTION

Physical and chemical characterizations are very important for a meaningful comparison of different liposome preparations or different batches prepared according to the same protocols. Both physical and chemical characteristics of liposomes influence their behavior in vivo and in vitro. As a rule, combinations of various characterization methods are used, as none of the existing techniques alone is able to describe liposomes adequately. Liposome characterization should be performed immediately after preparation. One should also ensure that no major changes occur on storage so that a well-characterized product is injected and the liposome dispersion warrants optimal reproducibility of clinical effects.

6.2 EXPERIMENTAL

6.2.1 Drugs and Reagents

Flutamide and 6-Mercaptopurine were kindly supplied as a gift sample by Coral Drugs Pvt. Ltd., New Delhi; and by Dabur Therapeutics Ltd., Ghaziabad, India, respectively; disodium hydrogen phosphate and potassium dihydrogen phosphate AR grade (S.D.fine chemicals, Biosar, Thane); sodium chloride AR grade (National Chemicals, Baroda); sodium lauryl sulphate, chloroform and methanol (AR grade) were purchased from S.D.fine chemicals, Biosar, Thane. Distilled Water prepared in laboratory.

6.2.2 Apparatus

Olympus microscope BX 40 (Olympus Optical Co. Lts., Japan); Malvern particle size analyzer (Malvem Master sizer 2000 SM, U.K.); Transmission electron microscope (Jeol, JSM-840 SEM, Japan); Mettler DSC 20 Differential Scanning Calorimeter (Mettler Toledo, Switzerland); Zetasizer H_{SA} 3000 (Malvern Instrument Ltd., UK); Laboratory centrifuge (Sigma, 3K30); Remi heating mantle and Remi magnetic stirrer 1 MLH (Remi Equipments, Mumbai), Shimadzu UV-1601 UV-Visible spectrophotometer (Shimadzu corporation, Japan), Advance DPX 200 dual probe ^{31}P-NMR and (Broker Inc., Switzerland) and High-pressure homogenizer (Microfluidizer, Avestin, Canada).

6.2.3 Characterization of liposomes

An attempt was made to characterize the conventional and sterically stabilized liposomes containing flutamide (FLT) and 6-Mercaptopurine (6-MP). It was envisaged that such characterization would help in gaining a deeper insight into the factors that affect the performance of these liposomes both *in vitro* and *in vivo*. The prepared conventional and sterically stabilized liposomes containing flutamide (FLT) and 6-Mercaptopurine (6-MP) were characterized for the following attributes.

6.2.3.1 % Entrapment efficiency

The entrapment of FLT and 6-MP studied using the method described in Chapter 5 in preparations of FLT and 6-MP liposomes. The effect of homogenization on % entrapment efficiency was also determined.

6.2.3.2 Electrolyte induced flocculation test

As discussed in Chapter 5, Preparation of liposomes (Section 5.3.2.4)

6.2.3.3 Morphology of liposomes by photomicrography

As discussed in Chapter 5, Preparation of liposomes (Section 5.2.5.2)

6.2.3.4 Particle size and particle size distribution

The mean particle size of the prepared liposomes was obtained by using Malvern particle size analyzer model SM 2000, which follows Mies theory of light scattering. Diluted liposome suspension was added to the sample dispersion unit-containing stirrer and stirred at 2000 rpm in order to reduce the inter particle aggregation, and laser obscuration range was maintained between 10-15%. The average particle size was measured after performing the experiment in triplicate. Table 6.1 shows the mean particle size of the various liposomal formulations before and after 3 cycles of homogenization at 15, 000 psi pressure. The particle size and distribution pattern of the FLT and 6-MP liposomal formulations after 3 cycles of homogenization is shown Figure 6.1 and 6.2.

6.2.3.5 Transmission Electron Microscopy

The liposomal dispersions were observed under a transmission electron microscope (Zeiss. EM 109). Copper grids, double coated with Formvar, and carbon were used to examine the samples. The liposomal dispersions were diluted five times with distilled water in eppendorf tubes with a 200-µL of distilled water using fixed micropipette. A drop of the diluted sample was placed on the coated side of the grid and kept settling for 5 min. The grids were then blotted on a filter paper and stained with aqueous phosphotungstic acid (1%) and kept for 3 min. The grids were then rinsed with distilled water to wash off the excess stain and dried at room temperature. The grids were then placed in the sample inlet chamber of the TEM and observed. A series of photographs were recorded avoiding overlap of the areas. The TEM micrographs of the FLT-SL and 6-MP-SL are depicted in Figure 6.3 and 6.4.

6.2.3.6 Zeta potential measurements

Zeta potential is a measure of dispersion stability and can be related to the surface charge of colloidal suspensions (303). The method uses the autocorrelation function of the light scattered in a colloid solution measured by a photon counting system. The particles move in an electric field of known strength in the interference pattern of two laser beams and produce scattered light, which oscillates in time in a way, which depends on the speed of the particles. The photo multiplier collects the light scattered by the particles and the measured autocorrelation function is first converted. using a Fourier Transform, into a frequency spectrum. The frequencies are then converted successively to velocities, electrophoretic mobilities and, finally, zeta potentials (304). The relationship of zeta potential to the particle velocity in a unit electric field (electrophoretic mobility) is described by the Henry equation

$$U_E = 2\epsilon f K_a z/6\pi\eta$$

where (U_E) electrophoretic mobility, (z) zeta potential, (ϵ) dielectric constant and (η) viscosity. $f(Ka)$ is a function of the electric double layer thickness and particle diameter. In aqueous media or moderate electrolyte concentrations (10 mM NaCl). $f(Ka)$ value is 1.5, which is used in the Smoluchowski approximation

$$U_E = \epsilon z/4\pi\eta$$

At 25 °C, the zeta potential can be approximated as (305)

$$Z = 12.85 U_E \, mV$$

Zeta potential was measured at 25 °C using a Zetasizer 3000 H_{AS} (Malvern Instruments Ltd., Malvern, U.K.) based on the method of photon correlation spectroscopy. An aliquot of 40 μl of liposomes was diluted in 20 mL of 10mMNaCl (pH 6.7) and the solutions were passed through a 0.2 μm syringe filter (Minisart, Sartorius, Germany). Samples were injected into the cylindrical couvettes and results were recorded. Before putting the fresh sample couvettes was washed with the methanol and rinsed using the sample to be measured before each experiment. Each sample was analyzed in triplicate.

6.2.3.7 Differential Scanning Calorimetry

Differential Scanning Calorimetric (DSC) thermograms of PC, HSPC, Cholesterol, FLT, 6-MP, FLT and 6-MP physical mixture as well as FLT and 6-MP encapsulated conventional and stealth liposomes were recorded on Mettler DSC 20 Differential Scanning Calorimeter (Mettler Toledo, Switzerland). The samples were weighed in perforated aluminum pans and scanned between 30-300°C at a heating rate of 10°C/min and nitrogen atmosphere. The scan was recorded and plotted showing heat flow (mV) on the Y-axis and temperature (°C) on the X-axis.

6.2.3.8 Lamellarity by ^{31}P-NMR studies

The liposome lamellarity was evaluated by ^{31}P-nuclear magnetic resonance spectroscopy (306) using an advance DPX 200 dual probe ^{31}P-NMR and (Broker Inc., Switzerland). Liposomal dispersion (50 μL) was diluted up to 100 μL with deuterated water (D_2O), introduced into the NMR sample tube and the spectra were recorded before and after the addition of Mn^{2+} (2 ml; 50 μmol of phospholipid per ml in an NMR tube in the form of manganese chloride ($MnCl_2$)) at levels high enough (5 mM) to eliminate the ^{31}P-NMR signal arising from those phospholipids facing the external medium. The spectra were recorded using 85% H_3PO_4 (phosphoric acid) as the reference standard. The average number of bilayers (N) was calculated from the

following expression: N = 100/(2 * RLOS), where RLOS is the percentage of the relative loss of signal found before and after Mn^{+2} addition (307).

6.3 RESULTS AND DISCUSSION

6.3.1 % Entrapment efficiency

The % EE of FLT and 6-MP in conventional and sterically stabilized liposomes was determined using the methods described in Chapter 5 (Preparation of liposomes, Section 5.2.5.1). Table 6.1 shows the results of these determinations.

Table 6.1: The % EE and mean particle size of the prepared liposomes before and after homogenization

Types of liposomes	Mole % of mPEG$_{2000}$-CC-PE	Particle Size (Mean ± SD)		% EE* after homogenization (Mean ± SD)
		Before homogenization	After homogenization	
FLT-CL	0	9.126±0.067	136.14 ±5.8	99.28±1.94
FLT-SL				
	3	10.928±0.055	146.68 ±3.94	98.81±2.36
	5	11.533±0.082	158.26 ±6.3	98.54 ±2.34
	7	12.103±0.07	218.2±6.73	94.62±2.48
	9	13.375±0.085	248.92±7.41	91.26±2.72
6-MP-CL	0	9.177±0.024	120.24±5.67	97.26±2.6
6-MP-SL				
	3	11.489±0.051	128.82±4.83	96.02±2.87
	5	12.57±0.042	132.26±4.61	96.38±4.5
	7	13.572±0.038	175.22±4.7	85.37±5.28
	9	15.84±0.057	201.57±6.91	77.39±4.67

*n=3

The maximum % EE of FLT and 6-MP in conventional liposomes was 99.28 ± 2.36 and 97.26 ± 2.6, respectively. It is expected because FLT and 6-MP are hydrophobic. For hydrophobic drugs, the entrapment in the lipid bilayer results in high values of entrapment whereas entrapment in the aqueous compartment is low particularly in multilamellar vesicles (308). The incorporation of steric stabilizing agent (mPEG$_{2000}$-CC-PE) in the bilayer does not cause any significant difference in drug entrapment up to 5-mole%. Significant differences are seen in the entrapment values of the liposomes when polyethylene derivative was of 7-mole % and 9-mole%

concentration. This may be due to the change in the hydrophobicity of the bilayer due to the addition of the polyethylene glycol into the lipid bilayer. The reduction in drug entrapment may also be due to the fact that both the drug and the polyethylene glycol were entrapped in the lipid bilayer. Further investigations into this aspect are required in order to satisfactorily explain the observed phenomena.

6.3.2 Electrolyte induced flocculation test

As discussed in Chapter 5, Preparation of liposomes (Section 5.3.3.2)

6.3.3 Morphology of liposomes by photomicrography

The photomicrographs of the prepared liposomes (Figures 5.1 and 5.13) indicate that the majority of the prepared liposomes were spherical and multilamellar before homogenization. Some unilamellar structures are also observed, the presence of which can be attributed to the sonication process used for size reduction of the prepared liposomes.

6.3.4 Particle size and size distribution

Table 6.1 shows the mean particle size of the prepared liposomes before and after homogenization. The sonication time of 20min was found to be adequate to reduce the size of the conventional liposomes of FLT and 6-MP to around 1-10 μm. Further reduction and rise in sonication time (10min and 30 min) yielded very high particle size liposomes. Hence the sonication time was fixed at 20min during the preparation of the liposomes. The liposomes were sequentially homogenized in high-pressure homogenizer (Microfluidizer, Avestin, Canada) for 3 cycles at 40°C for FLT liposomes and at 65°C for 6-MP liposomes, respectively because particle size could be reduced at phase transition temperature of lipid used. PC and HSPC were used as major lipids in preparation of FLT and 6-MP conventional and stealth liposomes. Phase transition temperature of PC and HSPC are 37°C and 62°C, respectively; therefore, the temperature during particle size reduction was maintained at 40°C for FLT liposomes and at 65°C for 6-MP liposomes, respectively. The resulting liposomes were of uniform particle size range of around 200nm, which is very important for *in vivo* biodistribution and tumor targeting.

The particle size of the sterically stabilized liposomes of FLT and 6-MP (Table 6.1) is greater than that of the conventional liposomes. It may be due to the increase in total weight of lipid as well as increase in rigidity of the bilayer of these liposomes due to the insertion of the sterically stabilizing agents like polyethylene glycol derivatives in the bilayer.

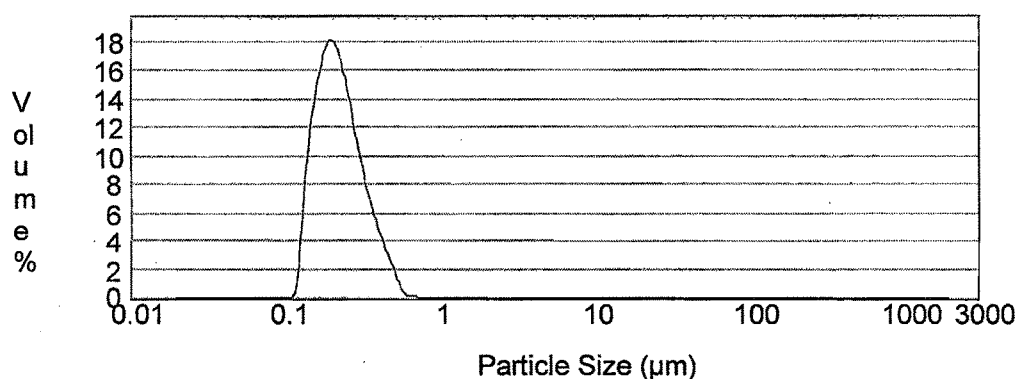**Figure 6.1: Particle size distribution pattern of FLT stealth liposomes after homogenization**

Particle Size (μm)

Figure 6.2: Particle size distribution pattern of 6-MP stealth liposomes after homogenization
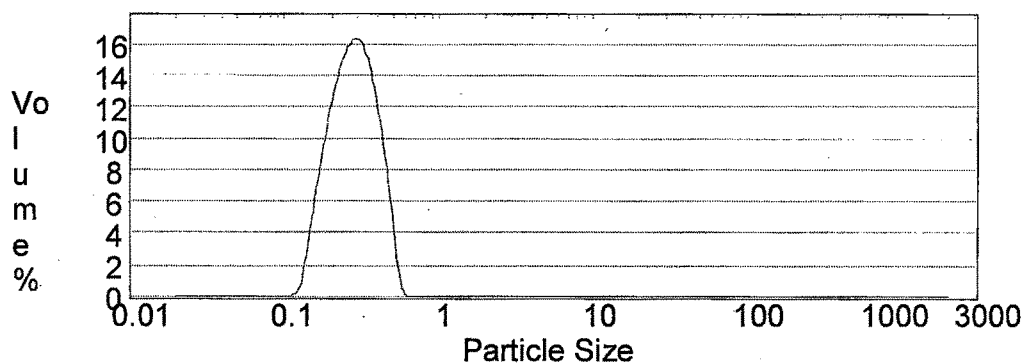
Particle Size

Figure 6.1and 6.2 show the particle size and distribution pattern of the FLT and 6-MP stealth liposomal formulations after three cycles of homogenization at 15, 000 psi pressure. The $d_{90\%}$ (diameter of 90% particles) of FLT and 6-MP liposomes was 209 nm and 274 nm as well as the span values ($d_{90\%}$-$d_{10\%}$/$d_{50\%}$) were of 0.89 and 0.74, respectively. Bell shaped curve of both liposomal preparations indicated that all liposomes had narrow particle size distribution.
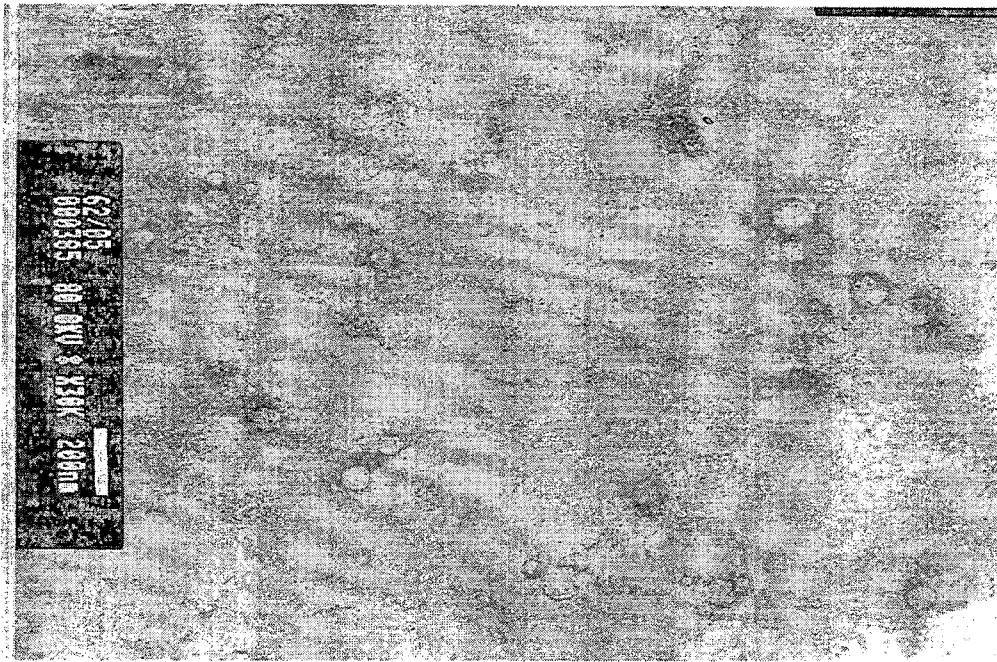
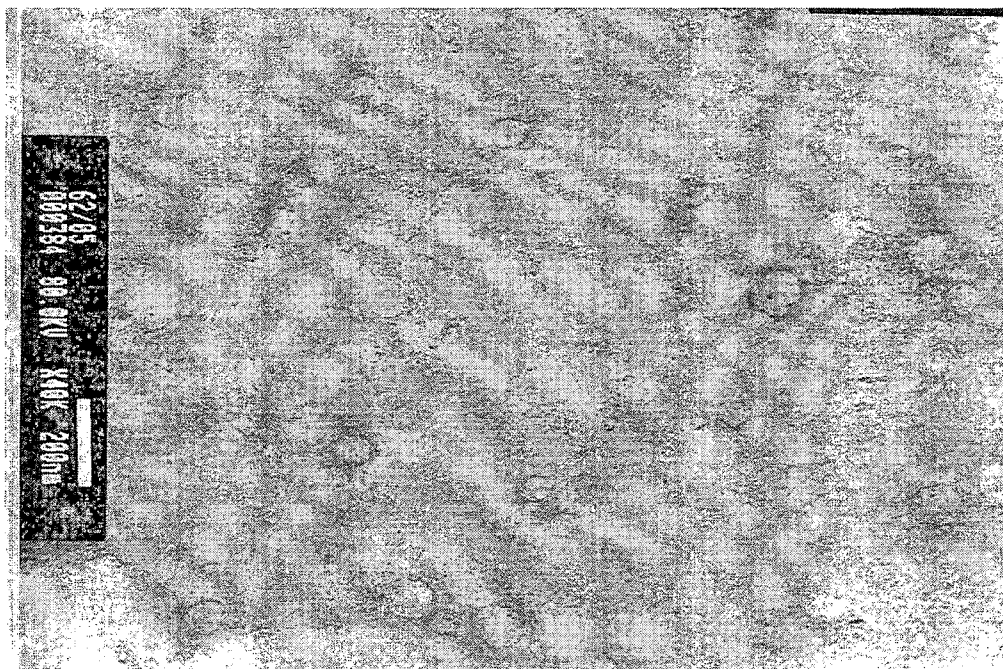**Figure 6.3: Transmission Electron Microscopic Photographs of FLT liposomes**

Figure 6.4: Transmission Electron Microscopic Photographs of 6-MP liposomes

6.3.5 Transmission Electron microscopic studies

TEM confirmed the formation of liposomes. The scanning of the grids showed the presence of spherical vesicles. The particle size of liposomes were below 200 nm, which was found suitable for in vivo studies, thus making it easily possible for liposomes to avoid from RES uptake. FLT-SL and 6-MP-SL were of spherical in shape as shown in Figure 6.3 and 6.4. Stealth liposomes with 5-mole% of $mPEG_{2000}$-PE was selected as the optimized batch as it also showed the highest entrapment efficiency and also gave an acceptable picture in TEM.

6.3.6 Zeta potential measurements

Table 6.2: Zeta potential and electrophoretic mobility of different liposomes based on their composition

Lipid composition (Types of liposomes)	Zeta potential (Z) mV	Electrophoretic mobility ($\mu m*cm/V*s$)
PC	-7.9	-0.624
PC: Chol (FLT Conventional liposomes)	-9.42	-0.733
PC: Chol: $mPEG_{2000}$-PE (FLT stealth liposomes)	-11.03	–0.89
HSPC	-6.7	-0.524
HSPC: Chol (6-MP conventional liposomes)	-7.28	-0.566
HSPC: Chol: $mPEG_{2000}$-PE (6-MP stealth liposomes)	-8.67	-0.674
HSPC: Chol: DSPG: $mPEG_{2000}$-PE	-22.4	-1.743

Table 6.2 presents the zeta potential and the electrophoretic mobility of the prepared liposomes. Inclusion of cholesterol into the liposome membrane caused a substantially higher negative zeta potential; this effect of cholesterol on the zeta potential is proportional to the mole percentage of cholesterol incorporated in liposomes for all compositions studied (EPC; EPC/Chol; HSPC; HSPC/Chol) and is in agreement with the results of Burner et al (309).

mPEG$_{2000}$-PE up to 5-mole% of total lipid in liposomes have a larger negative zeta potential than PC;HSPC or PC/Chol; HSPC/Chol liposomes. However, the effect of mPEG$_{2000}$-PE on the zeta potential of liposome negative charge is smaller than that of cholesterol, although both mPEG$_{2000}$-PE and cholesterol have identical phosphodiester groups. Incorporation of DSPG to 6-MP stealth liposomes further reduced the zeta potential.

6.3.7 Differential Scanning Calorimetry

DSC thermograms would be able to identify whether the agents are completely miscible with the components of the bilayer or not and was done with a view to understand the influence of insertion of steric stabilizing agent, in the bilayer, on the phase transition temperature of the system. The thermograms are shown as Figures 6.5and 6.6. Examination of the thermograms of the FLT and 6-MP stealth liposomes prepared using mPEG$_{2000}$-CC-PE showed that the agents introduced are completely miscible with the other components of the bilayer.

Figure 6.5: Thermograms of PC, pure FLT, Cholesterol, physical mixture and FLT stealth liposomes
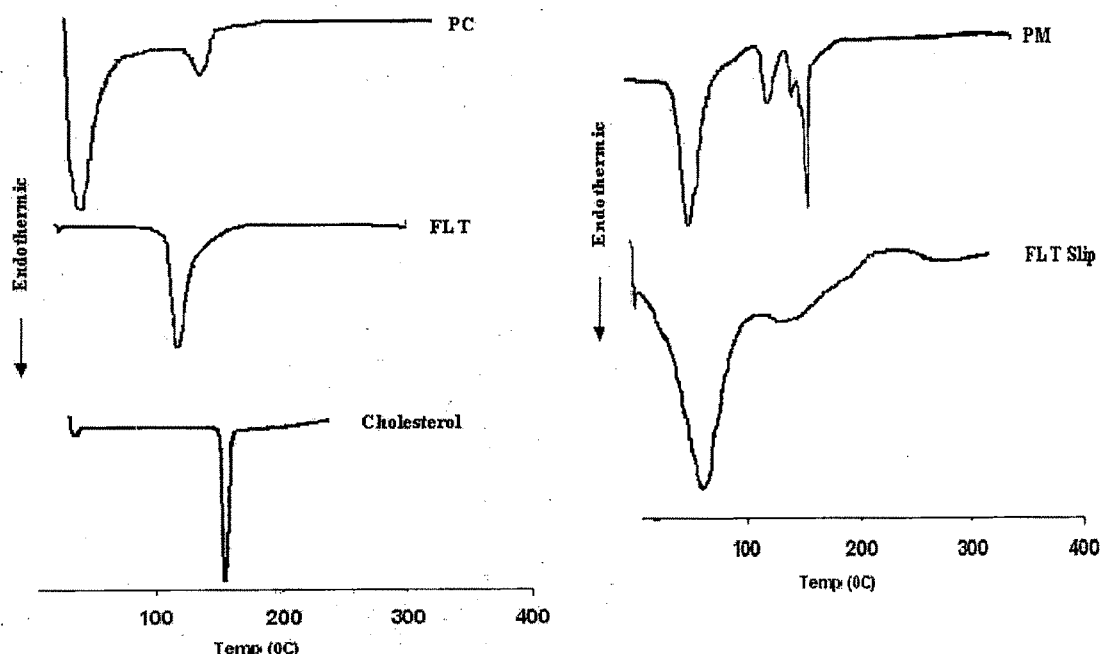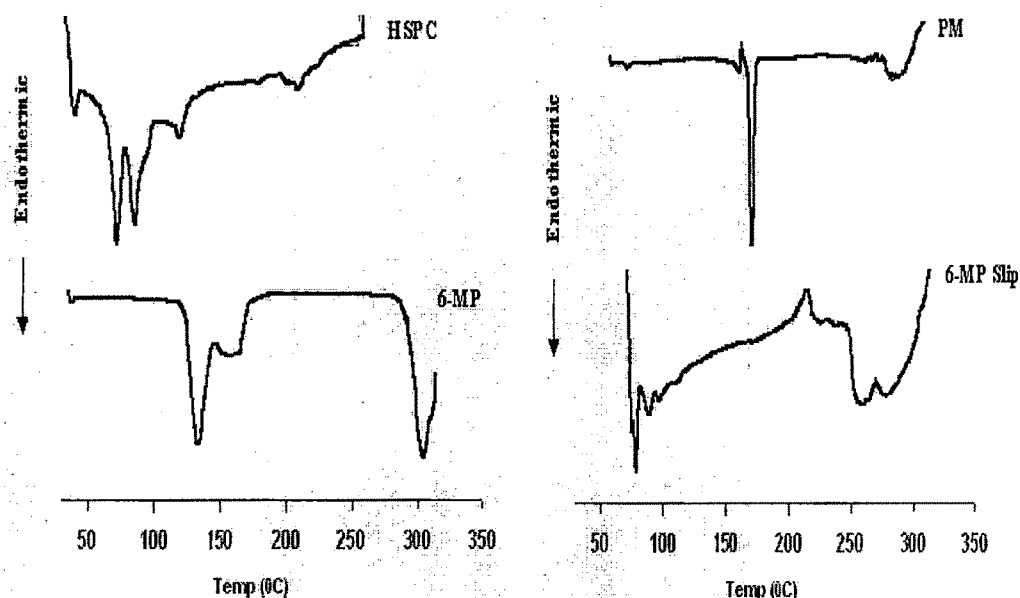
Figure 6.6: Thermograms of HSPC, pure 6-MP, physical mixture and 6-MP stealth liposomes

The DSC thermogram of FLT and 6-MP stealth liposomes show that phase transition temperature of the FLT and 6-MP liposomes lies between 32° to 37°C and 60° to 65°C, respectively. DSC thermogram of FLT and 6-MP stealth liposomes showed no melting endothermic peak of cholesterol at 150°C, which was found in thermogram of cholesterol. It also indicated that all the lipid components interact with each other to a great extent while forming the lipid bilayer. The thermogram of FLT and 6-MP shows endothermic peak at 110°C and 319°C, which was found broaden in the DSC thermogram of FLT and 6-MP liposomes, but the small endothermic peak was observed in a physical mixture.

6.3.8 Lamellarity by ^{31}P-NMR studies

^{31}P NMR spectroscopy gives the information on changes in the structure and dynamics of the polar choline heads of phospholipids of the model lipid membrane (310). Physical properties of model PC multilamellar membranes are the result of lipid–lipid interaction (as in a one component system). ^{31}P NMR spectra of PC membranes indicate an increase of motional freedom of polar head groups in a bilayer, where a phosphorous atom is located. Figure 6.7 shows the ^{31}P NMR spectra

of the FLT stealth liposomes before (A), after addition of $MnCl_2$ (B) and after homogenization (C).
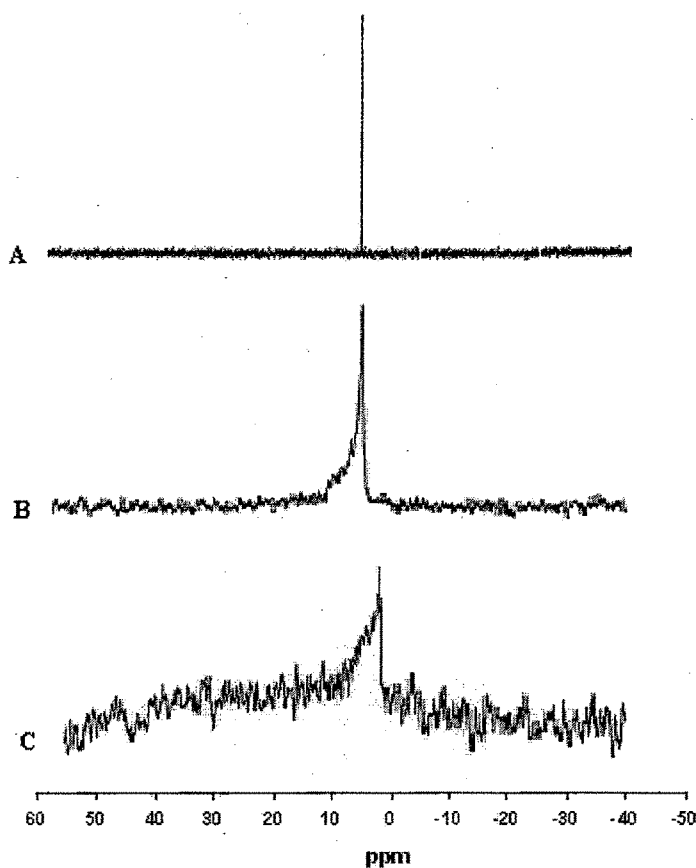

Figure 6.7: ^{31}P NMR spectra of the FLT stealth liposomes before (A), after addition of $MnCl_2$ (B) and after homogenization (C)

Phosphorus molecules in the phospholipids give characteristic NMR peaks. Upon addition of $MnCl_2$ in FLT stealth liposomes, the percentage of the relative loss of signal (RLOS) was found to be 15% (calculated as per equation 1, Chapter 6) indicated that flutamide liposomes were oligolamellar systems having more than 2 lamellae per vesicle. 20% RLOS was found after homogenization indicated that the number of lamellae per vesicle was reduced to two. Figure 6.8 describes ^{31}P NMR spectra of the 6-MP stealth liposomes before (A), after addition of $MnCl_2$ (B) and after homogenization (C). The ^{31}P NMR spectrum is a superposition of the broad anisotropic line characteristic for lamellar phase of phospholipids and a narrow isotropic line, typical for the phospholipids with isotropic mobility (311). The effect of broadening of ^{31}P NMR spectrum was observed in 6-MP stealth liposomes

because of spectrum was recorded below the temperature of main phase transition, which is indicative of change in chemical shift of anisotropy (312).
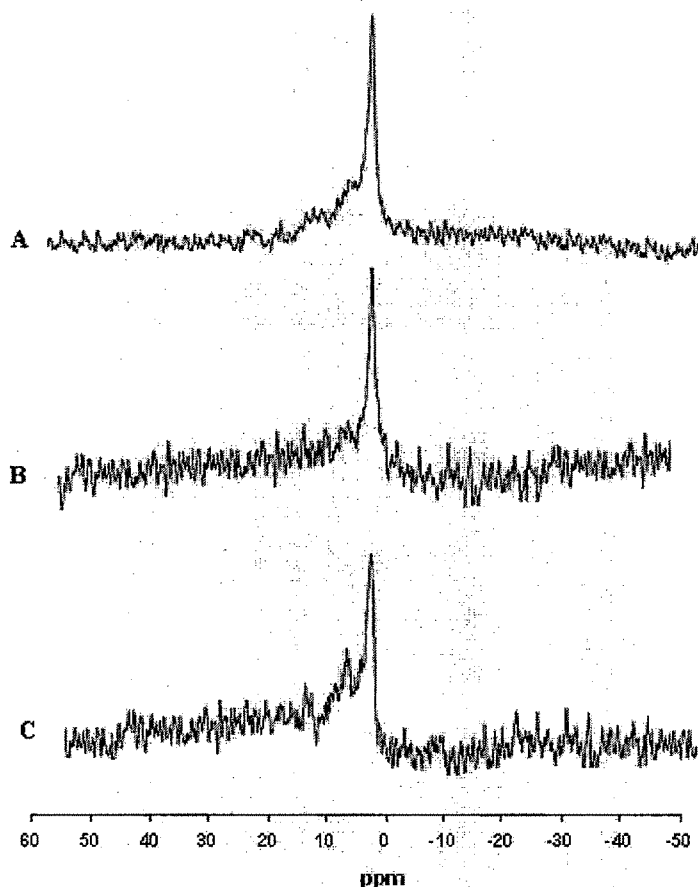

Figure 6.8: ^{31}P NMR spectra of the 6-MP stealth liposomes before (A), after addition of MnCl$_2$ (B) and after homogenization (C)

For PC based FLT stealth liposomes, chemical shift (δ value) was found 4.842 ppm at 30°C (phase transition temperature of PC) and 5.24 ppm at the same temperature in case of HSPC based 6-MP stealth liposomes (below phase transition temperature). Upon addition of MnCl$_2$ in 6-MP stealth liposomes, Mn^{+2} interacts with the outermost layer and broadens the peak and increased chemical shift value. The percentage of the relative loss of signal (RLOS) was found to be 10% (B) after addition of Mn^{+2} indicated that the hydration of the lipid films, followed by annealing, led to the formation of multilamellar systems with approximately five lamellae per vesicle. After passing 6-MP stealth liposomes from high pressure homogenizer with 3 cycle at 15,000 psi pressure (C), the number of lamellae per

vesicle was reduced to two (25% RLOS). Thus, a conversion from multilamellar to bilamellar systems after homogenization proves that the homogenization process also determined a significant reduction of the number of lamellae per vesicle.

6.4 CONCLUSION

Flutamide could be entrapped into CL and SL by thin film hydration technique with the % EE of 99.32% and 98.56%, respectively. The relatively narrow particle size distributions were achieved with an average particle size of CL and SL formulation was 136±5.8 nm and 158±6.3 nm after three cycle of homogenization. While in case of 6-MP liposomes, 97.26±2.6 % EE in CL with particle size of 120.24 ± 5.6 nm and 96.38±4.5 % EE with particle size of 132.26 ± 4.8 nm were obtained at 5-mole% of $mPEG_{2000}$-PE of total lipids in case of SL. The majority of the prepared liposomes were spherical and multilamellar before homogenization. The TEM studies show that the surface of the conventional and sterically stabilized liposomes does not show any visual difference. ^{31}P NMR studies showed that FLT liposomes were oligolamellar systems having more than two lamellae per vesicle after homogenization and 6-MP liposomes were bilayered. The zeta potential of FLT-CL and SL were -9.42 mV and -11.03 mV, respectively and 6-MP CL and SL were -7.28 mV and -8.67 mV, respectively indicating insignificant difference was observed after steric stabilization of liposomes by PEG in particle charge. In DSC studies, all the thermograms show a single-phase transition peak indicates that FLT and 6-MP were completely miscible with the components of the bilayer of liposomes.

6.5 CHARACTERIZATION OF MICROBUBBLES

Microbubbles are characterized for the following properties:

6.5.1 Experimental

6.5.1.1 Bubble size distribution and bubble number

The droplet concentration (bubble number) was measured using hemocytometer was calculated by red blood cells counting method. One drop of dispersion was applied on hemocytometer and a glass cover slip was carefully used to cover the sample before investigating the sample with a × 100 objective in Olympus (BX 40F4. Tokyo, Japan) microscope and bubbles per ml of samples were counted. The bubble size and size distribution of the microbubbles were measured using Malvern particle size analyzer (model SM 2000, Malvern, UK). Diluted microbubble suspension was added to the sample dispersion unit-containing a stirrer and stirred at 2000 RPM in order to reduce the inter bubble aggregation, and laser obscuration range was maintained between 10-15%. The average bubble size was measured after performing the experiment in triplicate. The bubble size of all prepared batches of all types of microbubbles are shown in Table 5.1-5.3, Chapter 5, Preparation of microbubbles. Figure 6.9-6.16 shows the bubble size distribution of all microbubbles. Table 6.3 shows the bubble size and number per ml of different types of microbubbles.

6.5.1.2 Surface morphology by photomicrography

The each dispersion of microbubbles was gently shaken and one drop was applied to the microscopic slide. A cover glass was carefully used to cover the sample before investigating the sample with a × 100 objective in Olympus (BX 40F4, Tokyo, Japan) microscope. All the selected batches of the prepared microbubbles were observed under Olympus (BX 40F4, Tokyo, Japan) microscope with a polarizing attachment to study their size and lamellarity. A photomicrography under 100X magnification is shown in Figure 6.17-6.19.

6.5.1.3 Gas content by densitometry

The content of gas (perfluoropentane) encapsulated within the microbubbles in the suspension samples was measured by densitometry method at 37°C. Initially, the weight of empty glass vial (X) was measured, vial was filled up to neck with

microbubble dispersion (P ml) and again weight was measured (Y). The density of microbubble before elimination of encapsulated gas (D_{int}) was calculated as

$$D_{int} = (Y - X)/P$$

The vial was kept in probe sonicator for 20 min and weight was measured (Z) and again density of microbubbles after elimination of encapsulated gas (D_{fin}) was measured as

$$D_{fin} = (Z - X)/P$$

The gas content in % v/v (C_{gas}) was calculated as

$$C_{gas} = [(D_{int} - D_{fin})/D_{fin}] * 100$$

The amount of gas encapsulated in each microbubbles is mentioned in Table 6.4.

6.5.1.4 Effect of sonication and centrifugation

There are various parameters reported to measure stability of microbubbles. Here two experiments were conducted: (a) the effect of sonication time and (b) the effect of centrifugation on bubble size and size distribution. For the sonication time study, samples were sonicated for 30 sec, 3 min and 5 min. For the centrifugation studies, microbubble solution 10 ml was transferred to a modified centrifuge tube. All samples were centrifuged at 300 RPM for 1 min, 300 RPM for 3 min and 500 RPM for 3 min. In most of cases, the solution separated into two distinct layers: (a) an upper layer containing mostly bubbles and (b) a lower layer containing suspended bubbles in aqueous media. The lower layer of the solution was collected for size and the top layer was discarded. If no distinct layer was observed, 5 ml was collected from the bottom of the centrifuge for bubble size analysis. Table 6.5 and Figure 6.20-6.21 represent the effect of sonication and centrifugation on bubble size distribution and bubble number of different types of microbubbles, respectively.

6.5.1.5 In vitro drug partitioning studies

If the microbubbles are prepared by method 3 (Mixing cum sonication technique (AALs)), the partitioning of drug in to the AALs and surrounding aqueous medium can be studied by spectrophotometrically. Indeed, 3 ml of AALs were layered on 10 ml of 30% and 90% sucrose gradient in a conical tube and centrifuged at 3000 RPM

for 10 min to force the AALs to the top and to remove oil and other materials not trapped in the AALs. Aliquots of both layers were taken and the amount of drug was estimated spectrophotometrically to confirm that the drug remained with the lipospheres layer and had not been pulled into the gradient with the other free materials. Table 6.6 represents the amount of drug pulled from AALs in different concentrations of sucrose solution.

6.5.1.6 Effect of different frequency ultrasound transducers

All three types of microbubbles were taken in test tube for controlled 2-MHz and 0.5 MHz ultrasound (US) exposure using respective ultrasound transducers probes. Each time the microbubbles were exposed to US for 30 sec. A hemocytometer was used to count the microbubbles per 10^{-4} ml. The hemocytometer was filled with microbubble suspension removed from test tube after US exposure (no US exposure for controls). Optical images of microbubbles were obtained using a × 100 objective in Olympus (BX 40F4, Tokyo, Japan) microscope. The total number of bubbles of all sizes was counted in 16 boxes present in each side of hemocytometer. The sample volume present in that particular area was 10^{-4} ml. The average number of bubbles was calculated for control, 0.5 MHz US exposed and 2 MHz US exposed bubbles. Figure 6.22, 6.23 and 6.24 represent photomicrography of MBs, GFMs and AALs without (sham exposed), exposed to 2 MHz US and exposed to 0.5 MHz US.

6.5.2 Results and Discussion

6.5.2.1 Bubble size and bubble number

Table 6.3: Bubble size and number of different microbubbles

Type of microbubbles	Bubble size in μm (Mean ± SD)				Bubble number $(X*10^7$ per ml) (Mean ± SD)
	$d_{10\%}$	$d_{50\%}$	$d_{90\%}$	Span	X
FLT-MBs	3.285	12.8	11.371	1.338	2.04 ± 0.048
6-MP-MBs	4.158	13.24	18.867	1.603	1.26 ±0.017
FLT-GFMs	4.09	9.0	21.737	1.798	1.23 ±0.018
6-MP-GFMs	3.838	6.9	17.454	1.633	1.29 ±0.029
FLT-AALs	4.596	7.5	20.006	1.628	1.26 ±0.022
6-MP- AALs	4.833	9.1	19.948	1.541	1.17 ±0.018
FLT-AALs*	0.140	0.193	0.283	0.740	0.97 ±0.014
6-MP- AALs*	0.178	0.280	0.428	0.890	0.86 ±0.019

* After homogenization for 3 cycles at 7,500 psi pressure

The mean diameter of all microbubbles was determined by Malvern particle size analyzer, which is shown in Table 6.3. Discussion is the same as described in section 5.3, Chapter 5, Preparation of microbubbles.

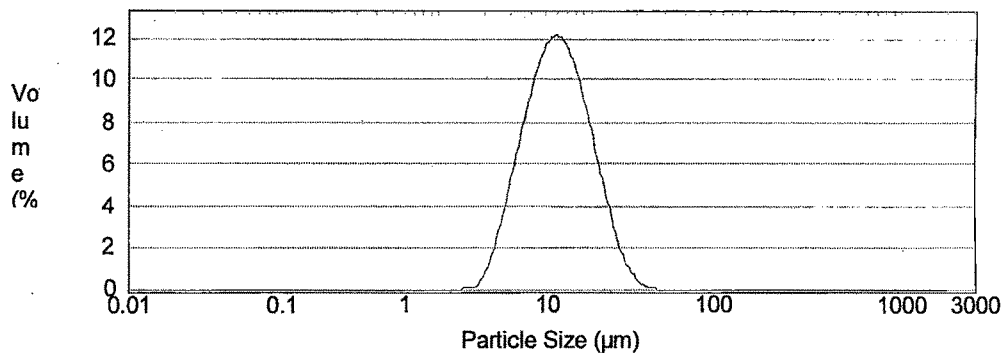**Figure 6.9: Particle size distribution pattern of FLT-MBs**

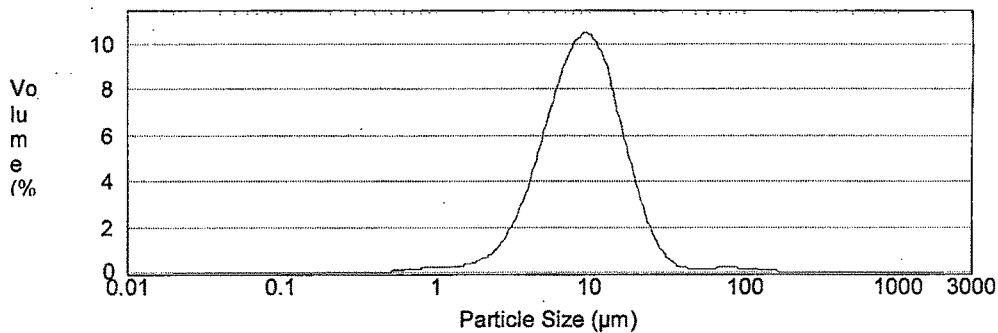**Figure 6.10: Particle size distribution pattern of 6-MP-MBs**

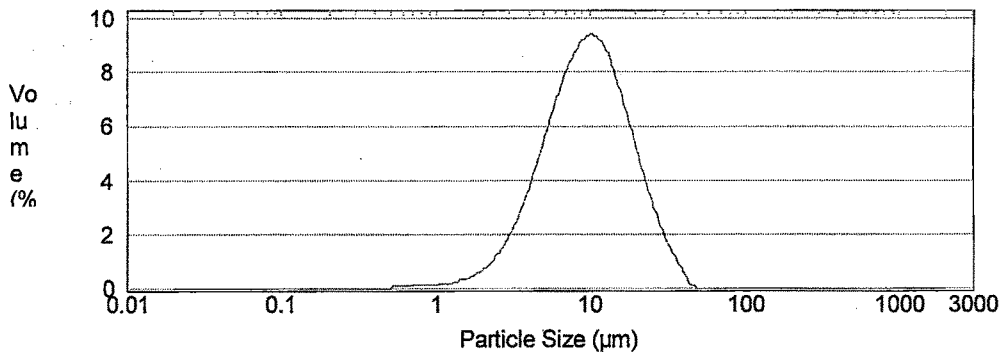**Figure 6.11: Particle size distribution pattern of FLT-GFMs**

Figure 6.12: Particle size distribution pattern of 6-MP-GFMs
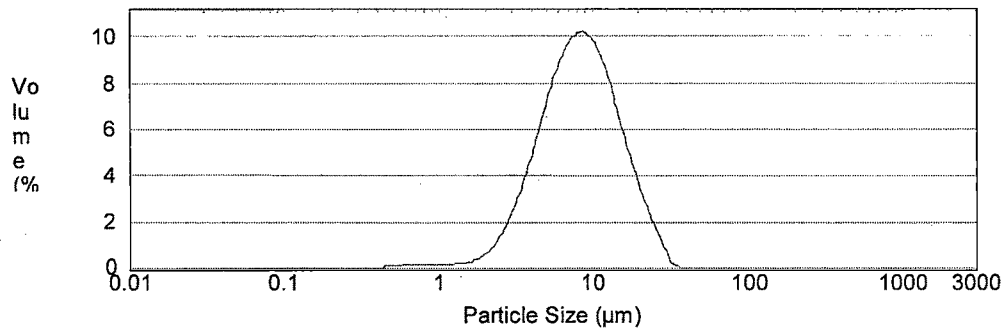

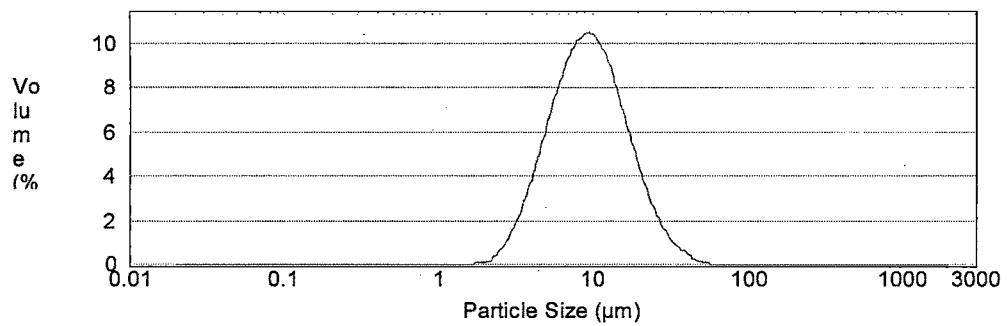**Figure 6.13: Particle size distribution pattern of FLT-AALs**

Figure 6.14: Particle size distribution pattern of 6-MP-AALs
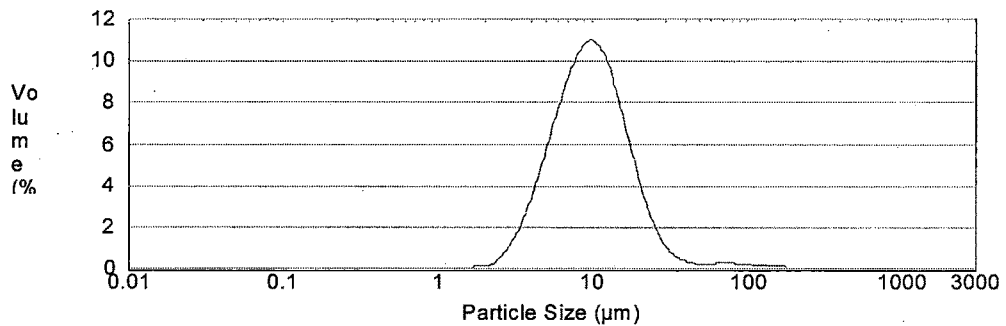

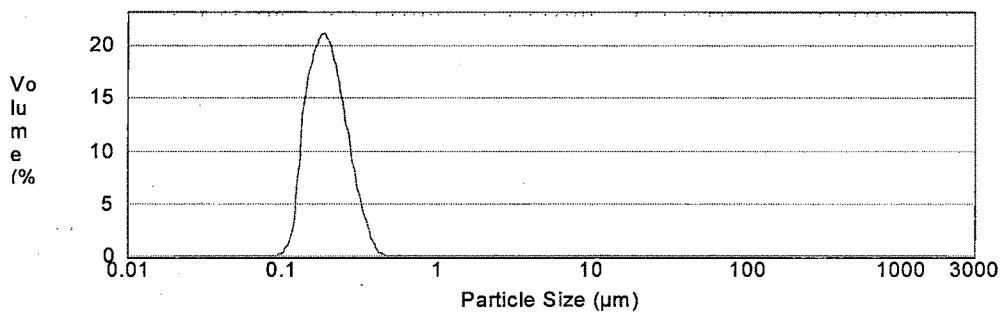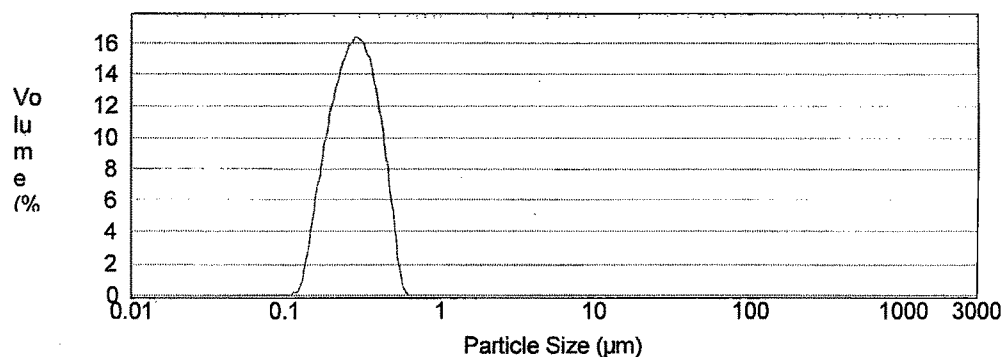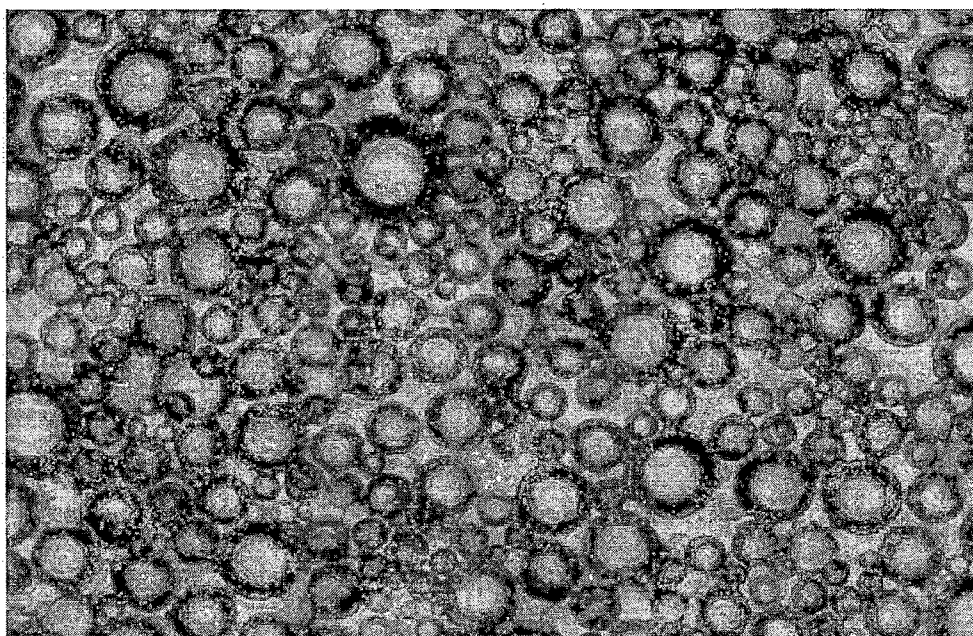**Figure 6.15: Particle size distribution pattern of FLT-AALs after homogenization**

Figure 6.16: Particle size distribution pattern of 6-MP-AALs after homogenization

6.5.2.2 Morphology by photomicrography

Figure 6.17: Microbubbles prepared by method 1 (MBs)

The close examination of the photomicrographs of the prepared microbubbles (Figure6.17, 6.18 and 6.19) indicates that the majority of the microbubbles were spherical, globular and raisin-shaped particles. The size of GFMs was less as compared to MBs and AALs, which may be attributed to sonication step involved in preparation of GFMs. Figure 6.18 showed that the AALs contained an outer wall surrounding a translucent ring-shaped region and an inner most spherical clear region. The oil layer appeared as yellow color surround a central microbubble.

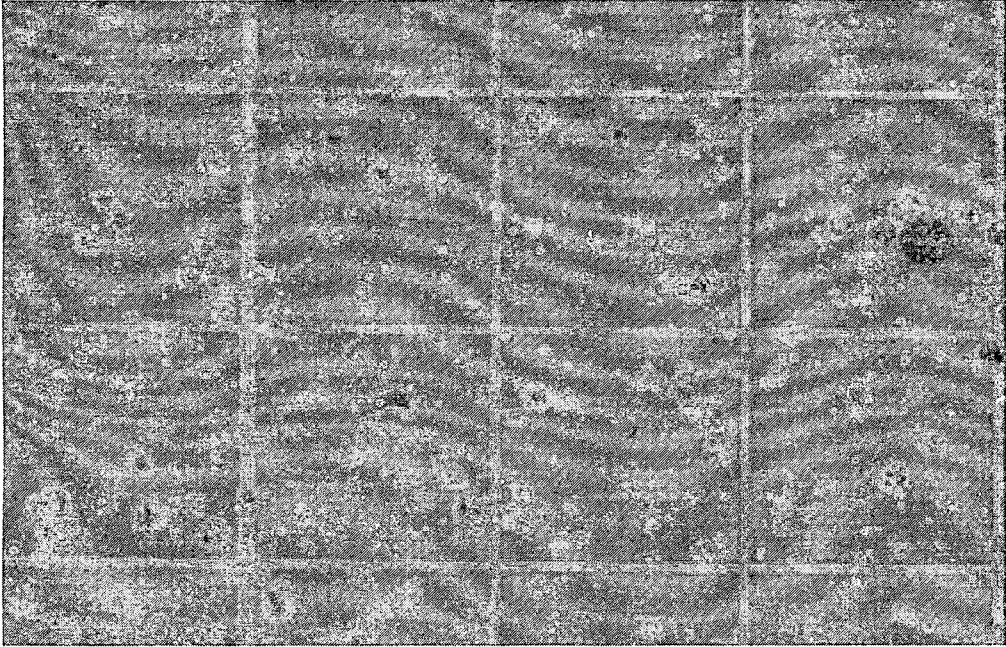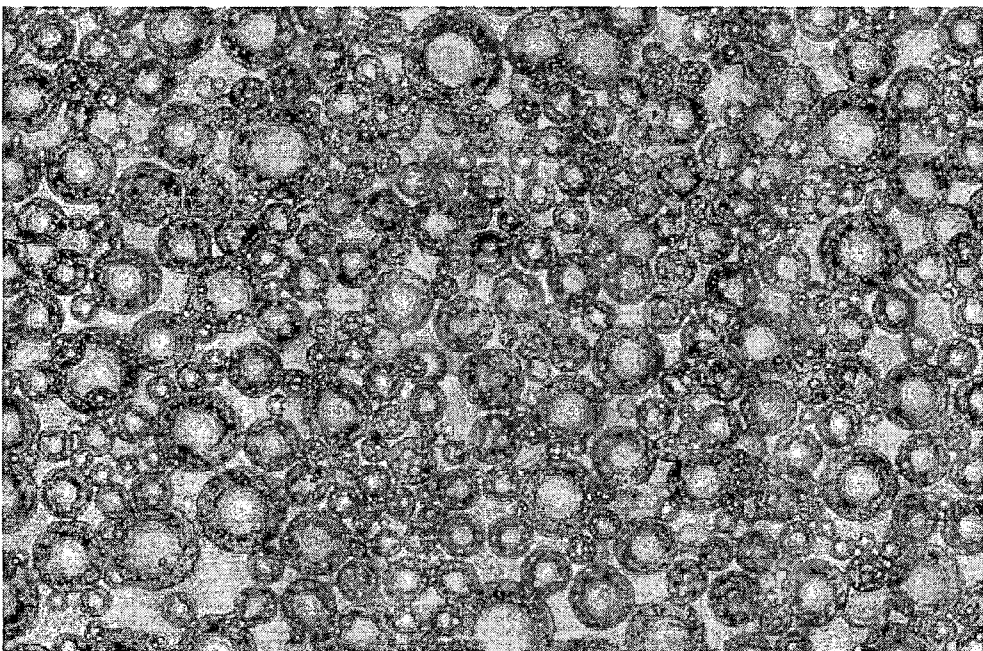**Figure 6.18: Gas-filled microparticles (GFMs)**

Figure 6.19: Acoustically active lipospheres

6.5.2.3 Gas content by densitometry

As seen from Table 6.4, the amount of gas encapsulated in each microbubbles was dependent on the ratio of perfluorocarbon gas added to the volume of aqueous phase added. The amount of gas encapsulated in different microbubbles varied from 0.89 to 4.02 % w/v. In the preliminary studies, as the amount of gas increased, the average shell size of the microbubbles was also increased until a critical size was reached (selected batches). The wall of microbubble no longer supported the structure above the mentioned concentration of gas, resulting in the collapse of the microbubbles.

Table 6.4: Composition and Gas content (% v/v) encapsulated in microbubbles

Batch No.	Drug (mg)	Drug/ Lipid Ratio	PFP (µl)	HSP C (mg)	mPEG 2000-PE (mg)	DSPG (mg)	OP (ml)	AP (ml)	Gas % v/v
FLT-MBs									
M27	5	1:10	150	41	4	5	5	10	1.38
6-MP-MBs									
M27	5	1:10	150	40	5	5	5	10	1.43

Batch No.	Drug (mg)	Drug: Polymer Ratio	Volume of PFP (µl)	NaCl Concentration (% w/v)	Gas content (% v/v)
FLT-GFMs					
GFM8	10	1:15	150	2	0.89
6-MP-GFMs					
GFM8	10	1:15	150	2	0.94

Batch No.	Drug (mg)	Drug: Lipid Ratio	PFP (µl)	PC (mg)	mPEG 2000-PE (mg)	DSPG (mg)	Oil (ml)	AP (ml)	Gas % v/v
FLT-AALs									
AAL2	5	1:10	450	41	5	4	2.5	5	3.61
6-MP-AALs									
AAL2	5	1:10	450	40	5	5	2.5	5	4.02

6.5.2.4 Effect of sonication on bubble size and number

To determine whether the sonication time has an effect on mean bubble size, the microbubble dispersions were sonicated for 30 sec, 3 min and 5 min. The average size of microbubbles was found in a range of 7.4-11.6 µm for the 30 sec sonication,

6.4-8.6 μm for 3 min and 5.3-6.8 μm for the 5 min sonication. Results are shown in Table 6.5.

Table 6.5: Effect of sonication time on bubble size and number of microbubbles

Type of formulation	Type of treatment	Bubble size in μm			Bubble No./ml
		$d_{10\%}$	$d_{50\%}$	$d_{90\%}$	
FLT-MBs	-	7.84	12.8	23.1	$2.04*10^7$
	30 sec sonication	7.26	11.62	20.57	$1.5*10^7$
	3 min sonication	5.102	7.23	12.72	$1.14*10^7$
	5 min sonication	4.03	6.115	10.53	$0.96*10^7$
6-MP-MBs	-	7.404	12.302	19.702	$1.26*10^7$
	30 sec sonication	5.503	9.915	14.43	$1.13*10^7$
	3 min sonication	5.102	7.602	12.32	$1.04*10^7$
	5 min sonication	4.702	5.319	10.02	$0.72*10^7$
FLT-GFMs	-	6.84	9.0	14.27	$1.23*10^7$
	30 sec sonication	6.23	8.426	12.543	$1.16*10^7$
	3 min sonication	5.92	7.63	11.49	$1.01*10^7$
	5 min sonication	4.786	6.482	10.23	$0.83*10^7$
6-MP-GFMs	-	5.621	6.92	12.53	$1.29*10^7$
	30 sec sonication	4.73	6.83	12.12	$1.14*10^7$
	3 min sonication	4.162	6.72	11.72	$1.03*10^7$
	5 min sonication	4.454	6.404	10.16	$0.86*10^7$
FLT-AALs	-	5.516	7.51	16.23	$1.26*10^7$
	30 sec sonication	4.982	7.461	14.235	$1.16*10^7$
	3 min sonication	4.429	6.93	12.42	$0.81*10^7$
	5 min sonication	4.126	6.835	9.873	$0.35*10^7$
6-MP-AALs	-	6.83	9.1	14.53	$1.17*10^7$
	30 sec sonication	5.981	8.32	13.92	$1.12*10^7$
	3 min sonication	5.638	7.796	11.358	$0.78*10^7$
	5 min sonication	4.435	6.82	9.863	$0.71*10^7$

In addition to having similar mean diameter after 5 min sonication, each preparation had somewhat similar size distributions as measured by Malvern bubble size analyzer with 90% less than 10 μm. It was also observed that the amount of microbubbles per ml was also affected by sonication time. The average bubble number per ml was $1.5-1.12*10^7$ after 30 sec, $0.78-1.14*10^7$ after 3 min and $0.38-0.96*10^7$ after 5 min of sonication found. Because little difference in mean size was noted, the amount of bubble number per ml between 3 min and 5 min was not large.

.Therefore, the sonication for 5 min was sufficient to reduce bubble size of all microbubbles in a range of 1-10 μm.

6.5.2.5 Effect of centrifugation on bubble size

There was noticeable decrease in mean bubble size measured as RPM and time for centrifugation increased. The initial mean size of MBs, GFMs and AALs, measured by Malvern bubble size analyzer as noted above, was 12.3-12.6 μm, 6.9-9 μm and 7.5-9.1 μm, respectively.
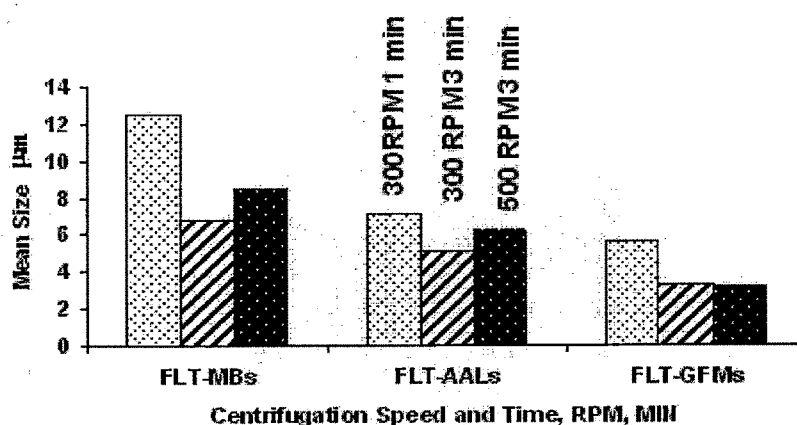
Figure 6.20: Effect of centrifugation on FLT bubble mean size
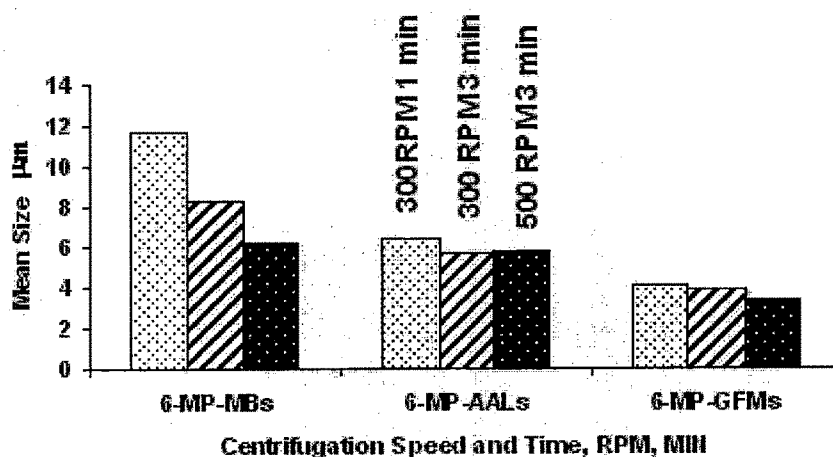

Figure 6.21: Effect of centrifugation on 6-MP bubble mean size

After centrifugation at 300 RPM for 1 min, the mean diameter for MBs, GFMs and AALs was in a range of 11.7-12.3 μm, 6.2-8.5 μm and 6.7-8.2 μm, respectively,

which gradually decreased to 4.1 to 5.6 μm, 3.16-3.26 μm and 3.3-4.1 μm. The data indicated that longer and faster centrifugation leads to reduced size microbubbles. The decrease in size because of centrifugation may be due to centrifugal force could be forcing gas out of the bubbles, creating bubbles with shells which are too closely packed at a molecular level, to maintain a stable shell. Alternatively, the smaller the bubble, the less could be its inherent stability and microbubbles could not remain stable longer times and higher speeds (more than 500 RPM). Therefore, centrifugation speed up to 300 RPM and time up to 3 min is more preferable to reduce size of microbubbles in a range between 1-10 μm. The AALs were more stable as compared to other microbubbles (MBs and GFMs) towards sonication and centrifugation. The oil may provide a dampening layer to stabilize the bubbles.

6.5.2.6 In-vitro drug partitioning measurements

Table 6.6: Drug partitioning in presence of different sucrose solutions

Batch No.	Drug (mg)	PFP (μl)	Aqueous Phase (ml)	Soyabean oil (ml)	% Drug partitioned (Mean ± SD)	
					30 % w/v	90 % w/v
FLT-AALs	5	450	5	5	0.58 ± 0.021	6.5 ± 0.22
6-MP AALs	5	450	5	5	0.75 ± 0.032	8.5 ± 0.37

The amount of drug partitioned from AALs to sucrose gradient was very less (6.5 % and 8.5 %) in both types of microbubbles. It indicated that the leakage of drug during, storage condition would be less. The drugs encapsulated in microbubbles will remain in oil phase as such for long period of time.

6.5.2.7 Effect of different frequency ultrasound transducers

Table 6.7 shows the microbubbles present per 10^{-4} ml. As shown in figure 6.22-6.24 and Table 6.7, the total number of surviving microbubbles after exposed to 5 MHz US is significantly lower than that after exposure to 2 MHz US.
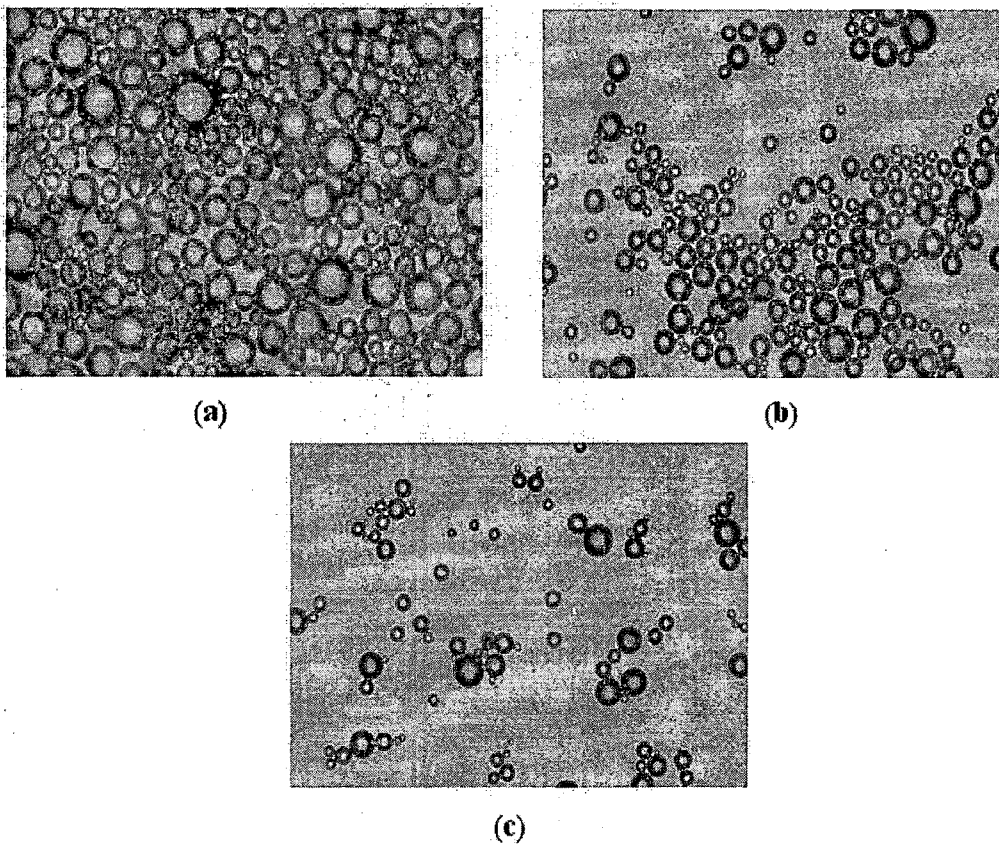
(a)

(b)

(c)

Figure 6.22: Photomicrography of (a) MBs without US exposure, (B) exposed to 2 MHz US and (c) exposed to 0.5 MHz US, respectively.

Table 6.7: Survival of microbubbles under different US exposure conditions

Type of microbubbles	Number of surviving microbubbles per 10^{-4} ml (Mean $\pm$ SD)		
	Sham exposed	0.5 MHz	2 MHz
FLT-MBs	193 ± 16	86 ± 9	132 ± 13
6-MP-MBs	187 ± 21	94 ± 13	148 ± 17
FLT-GFMs	200 ± 19	88 ± 11	140 ± 16
6-MP-GFMs	215 ± 23	109 ± 18	137 ± 15
FLT-AALs	161 ± 16	83 ± 9	139 ± 12
6-MP- AALs	187 ± 22	101 ± 16	131 ± 13

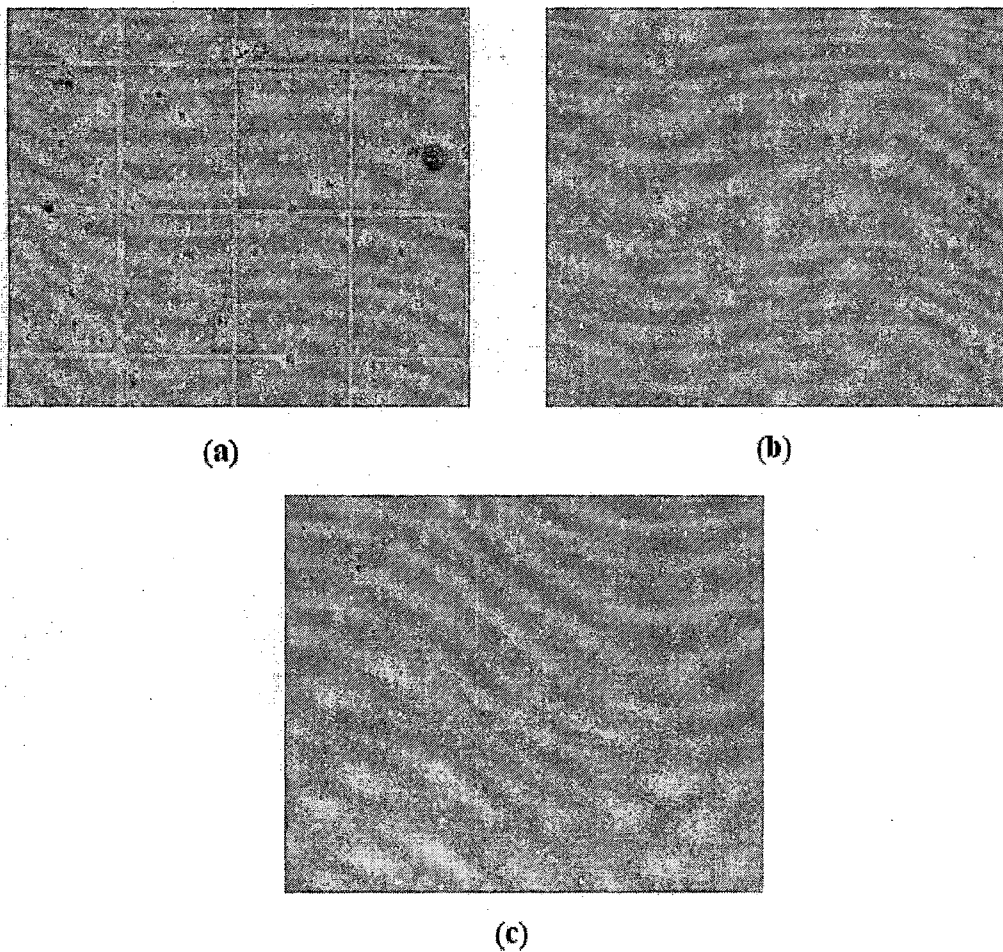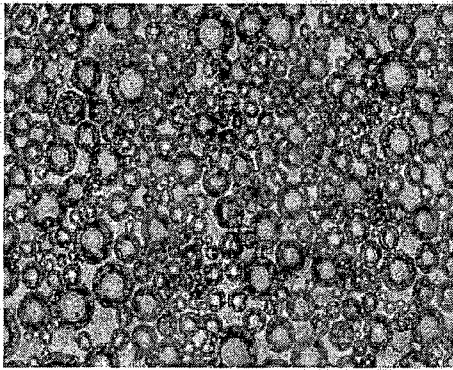(a)   (b)

(c)

Figure 6.23: Photomicrography of (a) GFMs without US exposure, (B) exposed to 2 MHz US and (c) exposed to 0.5 MHz US, respectively.

Figure 6.22-6.24 shows the typical optical images for the different types of microbubble suspensions. Each figure contains three optical images. They are the images for the sham exposed, exposed to 2 MHz US and exposed to 0.5 MHz US. The repetition period T of 2 MHz transducer is lower than that of 0.5 MHz transducer. In principle, lower T causes more US exposures per unit time. Thus, 2 MHz US should be more effective in disruption of microbubbles.
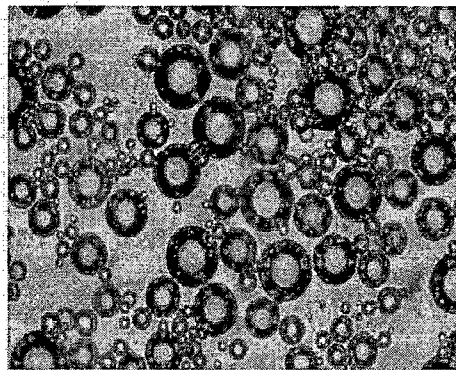
However, in reality, the 0.5 MHz US caused more bubble ruptures. Therefore, it is reasonable to conclude that frequency is the dominating factor. It may be useful in diagnostic and therapeutic application of microbubbles in US. This finding suggests that the low frequency US is more effective than high frequency US to disrupt the microbubbles. It may be due to generation of acoustic inertial cavitation force will be

more when microbubbles exposed to 0.5 MHz US than that of 2 MHz US. Therefore, low frequency US can penetrate deeper into soft tissue because its attenuation is lower.
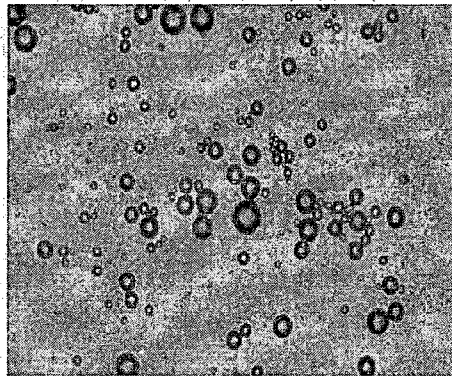
Figure 6.24: Photomicrography of (a) AALs without US exposure, (B) exposed to 2 MHz US and (c) exposed to 0.5 MHz US, respectively.

(a)

(b)

(c)